Han, Bing; Anwar Ul Haq, Rana; Louhi-Kultanen, Marjatta

# Lithium Carbonate Precipitation by Homogeneous and Heterogeneous Reactive Crystallization

*Published in:*
Hydrometallurgy

*DOI:*
10.1016/j.hydromet.2020.105386

Published: 01/08/2020

*Document Version*
Publisher's PDF, also known as Version of record

Hydrometallurgy 195 (2020) 105386

Contents lists available at ScienceDirect

Hydrometallurgy

journal homepage: www.elsevier.com/locate/hydromet

# Lithium carbonate precipitation by homogeneous and heterogeneous reactive crystallization

Bing Han[a,*], Rana Anwar UI Haq[b], Marjatta Louhi-Kultanen[a,*]

[a] School of Chemical Engineering, Aalto University, P.O. Box 16100, FI-00076 Aalto, Finland
[b] Outotec Oy, Rauhalanpuisto 9, FI-02230 Espoo, Finland

ARTICLE INFO

*Keywords:*
Carbon dioxide
Lithium carbonate
Precipitation
Recovery

ABSTRACT

Lithium carbonate precipitation from a $Li_2SO_4$ solution in a stirred crystallizer in semi-batch processes was investigated and compared using a heterogeneous $CO_2$ reaction and homogeneous $Na_2CO_3$ reaction. Nucleation and crystal growth were successfully monitored by an inline Particle Track based on the focused beam reflectance measurement technique. The results obtained indicate that the particle size decreased with an increase in mixing speed for both precipitation processes. However, the $CO_2$ feed rate in the heterogeneous reaction and the pumping rate of $Na_2CO_3$ in the homogeneous reaction did not have a significant impact on the particle size distribution. Temperature and the final pH play critical roles in precipitation when using $CO_2$ as a reactant. High alkaline conditions are needed to induce heterogeneous precipitation. The lithium recovery with homogeneous precipitation was higher than with heterogeneous precipitation, probably due to the gas-liquid mass transfer phenomena of absorption influencing carbon dioxide conversion to carbonate ions in heterogeneous precipitation. Agglomerates of leaf-shaped primary crystals were mainly obtained.

## 1. Introduction

Lithium demand has been boosted due to the high consumption in the lithium battery industry in the last decades. According to an EU report EU report, 2014 (Report on Critical raw materials for the EU. Report of the Ad hoc Working Group on defining critical raw materials), lithium exceeds the threshold for economic importance and is reaching the critical point for supply risk, as assessed by the Environmental Performance Index. Lithium batteries are good candidates for energy storage since lithium is the lightest metal producing the most energy-dense battery materials (Whittingham, 2004), which are ideally suitable for portable electronics and hybrid vehicles. Swain (2018) reported that the lithium price increased by 40–60% in 2016 worldwide. A large amount of lithium salts, currently accounting for up to roughly 65% of the worldwide lithium demand, is needed and this figure is expected to keep growing continuously (Flixer et al., 2018). However, this would require a major increase in mining and ore processing, which will lead to a non-sustainable outcome and enhance environmental pollution. Besides the usage of raw material, reuse and recycling of the secondary material is of considerable importance when addressing the circular economy, environment safety, and steady supply chain security. It is essential to recover and recycle lithium more efficiently from different sources to avoid a shortage of this critical metal. Waste electrical and electronic equipment (WEEE) such as mobile phones, computers and TV sets is dramatically growing due to the development of new technologies. Thus, WEEE is of great importance as a source of lithium through collection, recycling and recovery. Besides WEEE, spent brine, effluent, and side streams from industrial plants usually contain a certain amount of precious elements. In these applications too, attention should be paid to their recovery and reuse in order to develop cost- and energy-efficient methods and technologies.

In the literature, several authors have investigated the recovery of lithium. For instance, Xu et al. (2014) investigated the usage of saline lake waters as a feedstock for lithium recovery. The review published by Swain (2017) introduced the lithium recovery processes from brines. In our previous work, Han et al. (2018), we investigated the recovery of lithium carbonate by precipitation from an aqueous multicomponent solution simulating battery waste leachate. Precipitation results of lithium carbonate ($Li_2CO_3$) via homogeneous reactions with sodium carbonate as the reactant have been reported by many authors (Zhang et al., 1998; Nayl et al., 2017; Han et al., 2018). Recently, Zhao et al. (2019a) investigated the application of ultrasound to assist the precipitation of lithium carbonate from lithium-containing solution. The results showed that ultrasound significantly reduced the polymerization of $Li_2CO_3$ particles and promoted the dissociation of impurity ions. Technical grade $Li_2CO_3$ crystals can be efficiently recovered from low

* Corresponding authors.
*E-mail addresses:* hanbing0712@hotmail.com (B. Han), marjatta.louhi-kultanen@aalto.fi (M. Louhi-Kultanen).

https://doi.org/10.1016/j.hydromet.2020.105386
Received 31 October 2019; Received in revised form 20 March 2020; Accepted 29 May 2020
Available online 31 May 2020

concentrated lithium-containing solution. Lithium phosphate was recovered continuously by using solid $Na_3PO_4$ from the filtrate with a lithium concentration of 2 g/L after $Li_2CO_3$ precipitation, as reported by the same research group (Zhao et al., 2019b). The lithium recovery yield can be increased by the application of ultrasound.

Lithium carbonate is the most important lithium compound produced commercially and accounted for 60% of the market share of lithium-based commercial products in 2017 (Litio and Jimenez, 2018). Either in the literature or in industry, the precipitation of $Li_2CO_3$ using soda ash ($Na_2CO_3$) has been commonly used as the final step to produce $Li_2CO_3$ crystals in a hydrometallurgical process.

Carbon dioxide ($CO_2$) is one of principle greenhouse gases causing climate change. Chemical trapping, in which $CO_2$ is converted to stable carbonate salts, is one of the most promising methods for carbon capture and storage to minimize the environmental effects of industrial plants (Ferrini et al., 2009; Velts et al., 2011; Sun et al., 2012). A few studies (Matsumoto et al., 2009; Zhou et al., 2014) have reported the application of $CO_2$ to precipitate $Li_2CO_3$. Zhou et al. (2014) used a coupled reaction and solvent extraction process to produce $Li_2CO_3$ from LiCl and $CO_2$. The particle sizes of the formed $Li_2CO_3$ were distributed in two ranges. Nanoparticles were produced by microwave irradiation of aqueous $LiNO_3$ solution containing $CO_2$ microbubbles (Matsumoto et al., 2009). In industrial processes, $CO_2$ is generally used to convert insoluble $Li_2CO_3$ into soluble $LiHCO_3$ to further increase the final purity of $Li_2CO_3$. Alternatively, $CO_2$ is introduced into LiOH solution to form $LiHCO_3$, which on heating can be converted to high purity $Li_2CO_3$. (Meng et al., 2019). High energy consumption is needed in this process for the conversion. However, to the best of our knowledge, there has not been a study to compare the homogeneous reaction (using carbonate salt as a reactant) and heterogeneous reaction (using $CO_2$ as a reactant) for $Li_2CO_3$ precipitation. In the present work we focused on how homogeneous and heterogenous precipitation systems differ under the same mixing conditions and which operating conditions have the major influence on crystal product properties.

In the present work, semi-batch homogeneous and heterogeneous precipitation of $Li_2CO_3$ were carried out in a stirred reactor. Sulfuric acid is usually used in the leaching process in the mining industry, and there is a high amount of sulfate ion present in the industrial effluent. Therefore, $Li_2SO_4$ solution was used as the initial solution in the current research work to gain deeper understanding of the phenomenon and kinetics of the precipitation process, which could be considered for use in an industrial process to recover lithium. The aim of the present work was to compare the precipitation and reaction kinetics of lithium with the reactants of $Na_2CO_3$ solution and $CO_2$ gas in alkaline solution in various operating conditions in terms of residence time, mixing intensity, and precipitation temperature. According to recent news, new battery chemical plants will be constructed in Finland for the manufacture of nickel, cobalt, and lithium products. Therefore, the recovery of lithium from primary and secondary resources is of great importance for the circular economy and sustainability. Since crystallization can be utilized successfully as a separation method for recovering valuable elements, the findings from the current research work have considerable value and can be used as a reference for the development of new technologies for lithium recovery.

## 2. Materials and methods

### 2.1. Materials

Anhydrous lithium sulfate ($Li_2SO_4$, Alfa Aesar) with a purity of 99.7% (metal basis) was used as the main reactant. Sodium hydroxide pellets (NaOH, EMSURE for analysis, Merck Millipore) were used to prepare the NaOH solution. Carbon dioxide gas ($CO_2$, 99.7%, AGA) was used as a reactant for the heterogeneous precipitation of $Li_2CO_3$. Deionized water was used to prepare different aqueous solutions. Anhydrous sodium carbonate ($Na_2CO_3$, EMSURE for analysis, Merck Millipore) was used as a reactant in homogeneous precipitation.

### 2.2. Experimental set-up and procedure

In the present work, semi-batch precipitation of lithium carbonate was investigated by homogeneous and heterogeneous reactions in a stirred, jacketed crystallizer.

#### 2.2.1. Heterogeneous precipitation

In the heterogeneous reaction study, $CO_2$ gas was fed as the carbonate source into the $Li_2SO_4$ solution to precipitate $Li_2CO_3$. In each experiment, 300 mL of $Li_2SO_4$ solution was prepared with a Li concentration of 20 g/L. It was noticed that the solution was turbid to some extent after mixing the $Li_2SO_4$ powder and deionized water. Thus, pretreatment was needed before the precipitation process. A clear $Li_2SO_4$ solution was obtained by vacuum filtration with a Büchner funnel (filter paper Grade 50, Whatman). Then, the clear solution was put into the jacketed glass reactor. A thermostat (Lauda ECO RE630), with an external temperature sensor immersed into the solution, was used to control the temperature of the solution through the jacket. A Rushton turbine with six blades was used for mixing and four baffles were symmetrically set in the inner wall of the reactor to prevent vortex formation during the mixing. The $CO_2$ gas was introduced by a metal gas feed tube with a sparger placed on the bottom of the reactor. The sparger was made of Teflon and had eight holes with a diameter of 1 mm. The eight holes line towards the bottom of the reactor in order to prevent any blockage by the precipitates. In each semi-batch experiment, 100 mL of NaOH solution with a concentration of 5 mol/L was added to the $Li_2SO_4$ solution at the beginning. When the solution temperature reached the target temperature and was kept constant for at least 10 min, feeding of $CO_2$ was started and its volume flow rate was adjusted with a rotameter to induce precipitation. The conductivity and pH of the solution were monitored with a Consort Multi-parameter analyzer (C3050). In some precipitation experiments, an inline probe (Particle Track G400, Mettler Toledo) was placed into the reactor and used to measure the count rates of various chord length size fractions to obtain kinetic data on the precipitation. The Particle Track measurement technique is based on Focused Beam Reflectance Measurement (FBRM). A laser beam passes through a set of optics and focuses on a tight beam spot in the sapphire window. The optics rotate at a fixed speed of 2 m/s to scan the flow of particles through the window. It provides precise and highly sensitive chord length data collection to capture real-time changes. All the heterogeneous experiments were carried out at 25 °C and 50 °C with different gas flow rates and mixing rates. Fig. 1 shows the experimental set-up for heterogeneous precipitation.

#### 2.2.2. Homogeneous precipitation

In the homogeneous reaction study, sodium carbonate was used as a reactant. A solution of 300 mL of pre-treated $Li_2SO_4$ solution with a Li concentration of 20 g/L was placed in the same reactor as the one used for heterogeneous precipitation. All the homogeneous experiments were only carried out at 50 °C. This is due to the lower solubility of $Na_2CO_3$ at 25 °C compared to 50 °C (CRC Handbook of Chemistry and Physics, 2010); more than 1 L of saturated $Na_2CO_3$ would be needed to precipitate $Li_2CO_3$ in the maximum amount at 25 °C, which was unrealistic for the present work. Furthermore, as the solubility of lithium carbonate in pure water is lower at 50 °C ($c^* = 1.07$ wt%) than at 25 °C ($c^* = 1.28$ wt%) (CRC Handbook of Chemistry and Physics, 2010), the crystal yield can be expected to be higher at 50 °C. Therefore, a higher crystal yield at 50 °C than at 25 °C with the model solutions was also verified in the preliminary studies of the present work. In each homogenous precipitation experiment, 102 mL of saturated $Na_2CO_3$ solution at 50 °C was prepared in a jacketed glass vessel controlled by a thermostat in advance. Then, it was pumped with a peristaltic pump (MasterFlex L/S, Cole-Parmer) through a metal tube into the $Li_2SO_4$

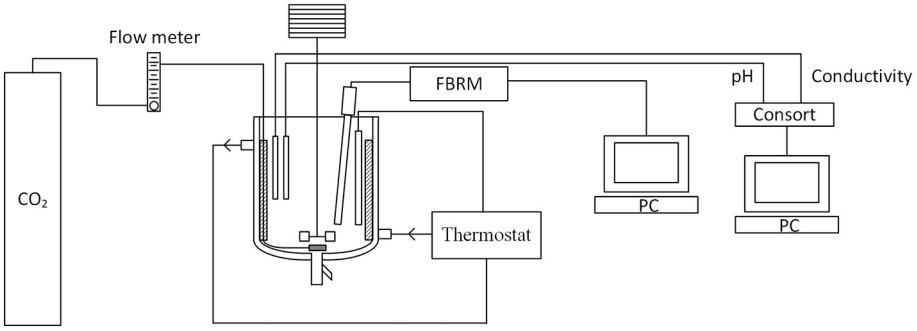


**Fig. 1.** Experimental set-up for heterogeneous precipitation of $Li_2CO_3$.

solution to precipitate $Li_2CO_3$. The inlet of the feeding tube was located at the same level as the impeller and pointed directly towards the center of the reactor. The tube used for the peristaltic pump was isolated with insulation material. A study was made of the influence of different variables, including the stirring rate and feed rate, on the properties of the product crystals.

### 2.3. Characterization

After heterogeneous and homogeneous precipitation, the solid sample was separated by vacuum filtration with a Büchner funnel. The crystals were dried in an oven at 50 °C at least overnight prior to solids analyses. The crystals were characterized by X-ray powder diffraction (XRD, X'Pert PRO) using a cobalt radiation source ($\lambda_{Ka1}$ = 1.7890 Å) operated at 40 kV with 40 mA. Scans were made over a 2θ range of 20–80° with a step size of 0.0263°. The morphology of the crystals was imaged using a Tabletop microscope (Hitachi TM4000plus). A particle size analyzer (Malvern Mastersizer 2000) was used to check the particle size distribution (PSD) of the final crystals. Pure ethanol (99.9%, ALTIA Oyj) was used as a background solvent for PSD analysis since $Li_2CO_3$ is insoluble in ethanol. The crystal yield was determined from the mass of the precipitates.

## 3. Results and discussion

### 3.1. Heterogeneous precipitation

#### 3.1.1. Effect of gas flow rate

From the pH measurement it was noticed that the initial pH of the solution varied to some extent due to the presence of impurities in the $Li_2SO_4$ chemical. Energy dispersive spectroscopy analyzed the precipitates on the filter paper and showed that Fe and Si were probably the main impurities. According to our records, the pH of the initial solution after adding soda was in the range of 10.92–11.90 at 25 °C, and in the range of 9.18–10.56 at 50 °C. Fig. 2 shows the pH and conductivity changes as a function of time for different gas flow rates and temperatures at a mixing rate of 500 rpm. It can be seen from Fig. 2a that the pH slightly decreased at the beginning (first pH period), then reduced rapidly to the target pH (second pH period), and remained almost constant during the aging period (third pH period).

A solution of NaOH was added to make the initial solution alkaline. When $CO_2$ (g) was fed into the alkaline solution, the $CO_2$ (g) absorbed into the aqueous NaOH solution, forming $CO_2$ (aq), as presented in Eq. (1). Subsequently, $CO_2$ (aq) reacted with $OH^-$ to form $HCO_3^-$ and $CO_3^{2-}$ ions, as shown in Eqs. (2) and (3), respectively. Therefore, the pH slightly decreased during the first pH period. When a certain amount of $CO_3^{2-}$ (aq) was formed and reached the supersaturation degree of $Li_2CO_3$ together with the $Li^+$ concentration in the solution, $Li_2CO_3$ crystals started to precipitate. This reaction is shown in Eq. (4). The reduction rate of the pH accelerated as well, due to the consumption of $CO_3^{2-}$ ion. As observed with the naked eye, the solution started to become unclear already in the first pH period. This is consistent with the results obtained from the FBRM signal. As shown in Fig. 3a, the count rates below 10 μm (blue curve) started to increase at around 11 min, which clearly indicates the formation of nuclei. The pH decreased rapidly to the target pH in the second pH period. This means that more $OH^-$ in the solution was consumed. Since $CO_2$ was continuously fed to the solution, it reacted with water so that the pH decreased continuously. Finally, when the $CO_2$ feed was stopped, the pH and conductivity remained at a constant level in the third pH period. From the conductivity curve, it can be seen that it decreased continuously from the beginning to the end of the initial period before the pH dropped rapidly, and then it maintained a constant level at the end of the semi-batch precipitation process. The formation of $Li_2CO_3$ crystals decreased the electrical conductivity.

$$CO_2(g) \rightarrow CO_2(aq) \quad (1)$$

$$CO_2(aq) + OH^-(aq) \rightleftharpoons HCO_3^-(aq) \quad (2)$$

$$HCO_3^-(aq) + OH^-(aq) \rightleftharpoons H_2O(l) + CO_3^{2-}(aq) \quad (3)$$

$$2Li^+(aq) + CO_3^{2-}(aq) \rightarrow Li_2CO_3(s) \quad (4)$$

As seen from Fig. 2, the decrease in pH in the second pH period occurred earlier with the higher gas flow rate at both temperatures of 25 °C and 50 °C. The conductivity also decreased faster with the higher gas flow rate of 0.5 L/min in comparison with the lower flow rate of 0.3 L/min. This indicates that, with the higher gas flow rate, the reactant feed rate is greater leading to higher supersaturation and thus enhancement of the precipitation process.

The precipitates obtained from the precipitation experiments were analyzed with a laser diffraction particle size analyzer and the results are shown in Fig. 4. It can be seen that the $CO_2$ flow rate did not have a significant impact on particle size distribution at a rotation speed of 500 rpm for both temperatures of 25 and 50 °C. A minor difference could be observed in the particle size distribution at a mixing rate of 600 rpm. At 50 °C, larger particles were obtained with the higher flow rate. This can be explained by the fact that nucleation occurred earlier with the higher gas flow rate, which promoted crystal growth. This result is consistent with the results obtained from previous research on magnesium carbonate precipitation (Han et al., 2014). At 25 °C, however, particles obtained with the lower gas flow rate were slightly larger than those obtained with the higher flow rate, and there were also a small amount of very small particles (< 10 μm), as indicated in Fig. 4. This may be because nucleation continued even though the $CO_2$ had stopped as the precipitation did not reach equilibrium, as verified by the FBRM results (a detailed discussion can be found in Section 3.1.2).

#### 3.1.2. Effect of temperature

The changes in pH and conductivity as a function of time at 25 °C were discussed in Section 3.1.1. When comparing the results obtained at 25 °C and 50 °C, the corresponding three periods of pH curves can be seen in Fig. 2a and b. Slight differences can be seen for the initial pH

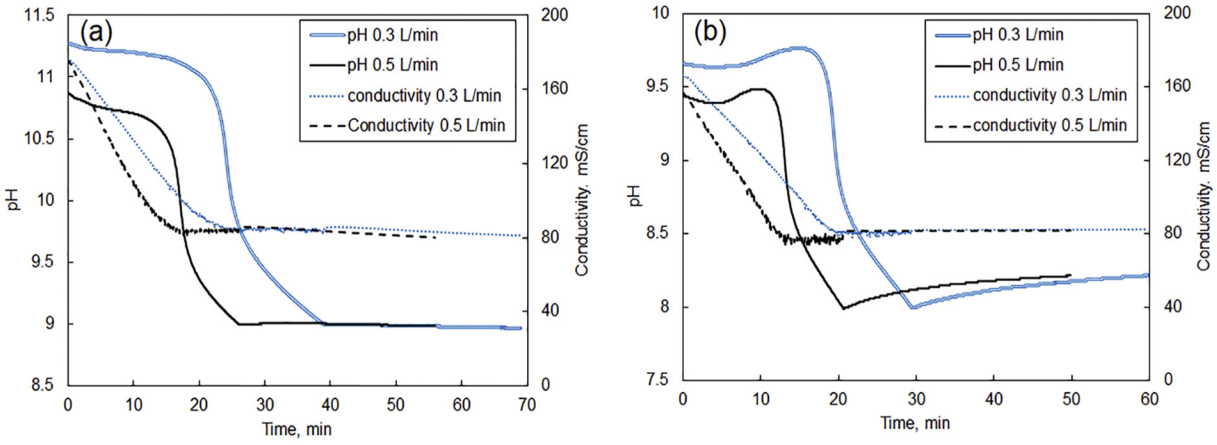


**Fig. 2.** Changes of pH and conductivity profiles as a function of time at a mixing rate of 500 rpm for different $CO_2$ gas flow rates at 25 °C (a) and 50 °C (b) in the $Li_2CO_3$ precipitation process.

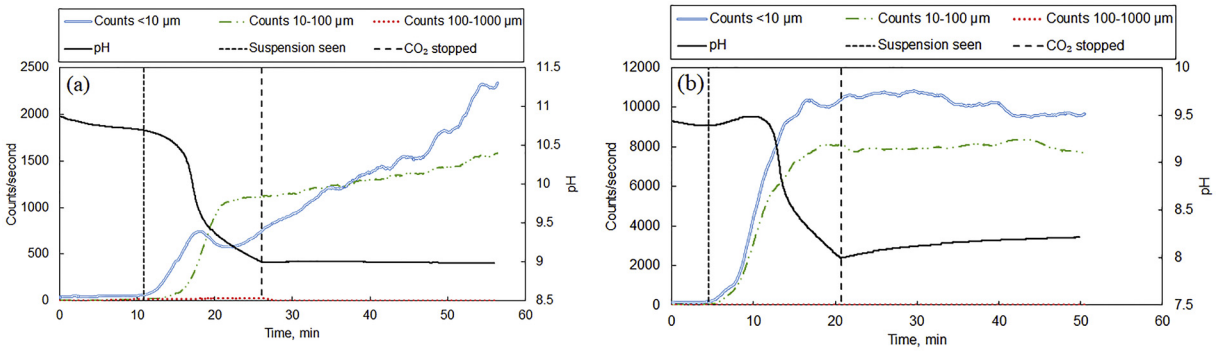


**Fig. 3.** Focused beam reflectance measurement (FBRM) signal and pH trends over time at a mixing rate of 500 rpm and $CO_2$ flow rate of 0.5 L/min at 25 °C (a) and 50 °C (b).

period and final period, where the pH increased slightly before it suddenly dropped and rose slightly at the end. These need to be further studied to understand the mechanism of the process.

Higher temperature leads to faster reaction and promotes the progress of precipitation. Supersaturation was higher at 50 °C due to the lower solubility of $Li_2CO_3$. This can clearly be seen from the FBRM results shown in Fig. 3. The count rates of small particles (< 10 μm) were still increasing when the experiment ended at 25 °C, whereas they were slightly reduced at 50 °C. This means that nucleation still continued after stopping the flow of $CO_2$ at 25 °C. Regarding 50 °C, after stopping the $CO_2$ feed, the reactions were almost completed and crystal growth may still have taken place until the system reached the steady state. It can be clearly seen from the count rates of the 10–100 μm size fraction that a constant level was maintained and the count rates of the smallest size fraction decreased simultaneously. Moreover, nucleation and crystal growth rates were significantly increased at 50 °C, and according to the FBRM signal, the count rates of the < 10 μm and 10–100 μm size fractions at 50 °C were several times higher than those at 25 °C.

To prove the findings we made, a separate precipitation experiment was carried out at 25 °C with a mixing rate of 500 rpm and flow rate of 0.3 L/min. In this experiment, the $CO_2$ was stopped when the count

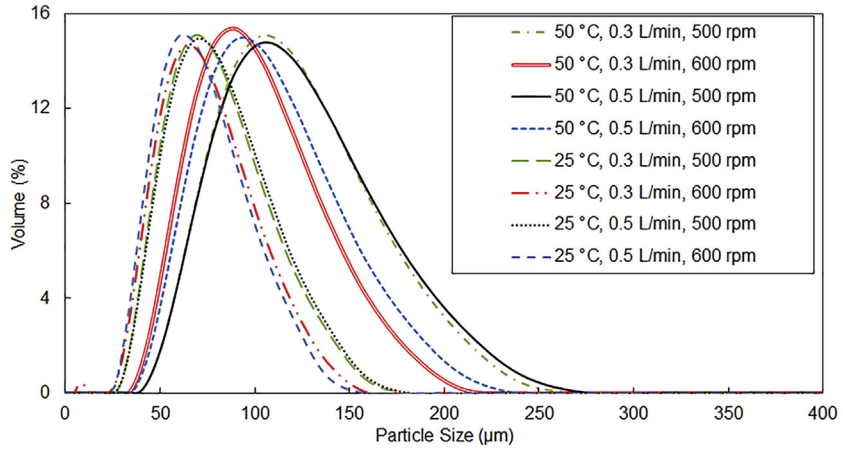


**Fig. 4.** Particle size distribution of $Li_2CO_3$ obtained from various temperatures, mixing rates, and $CO_2$ flow rates in the heterogeneous precipitation process.

rates (< 10 μm) obtained from FBRM were becoming constant. In this case, the pH ended at 8. After stopping the $CO_2$, the pH slightly increased in a similar way as the pH trend at 50 °C for the stability period. The total experiment time was about 102 min. This indicates that the time needed to achieve equilibrium at 25 °C is much longer than that at 50 °C. Moreover, an inline FBRM probe is a good and useful tool to monitor the real-time dynamic phenomena of precipitation processes. If inline Raman spectroscopy can be used in future work, the mechanism and kinetics can be fully understood since it is capable of monitoring different ions in the reaction and tracking the changes of solids in the precipitation process (Han and Louhi-Kultanen, 2018).

It can be clearly seen from Fig. 4 that the particle size of $Li_2CO_3$ precipitated at 50 °C is larger than that precipitated at 25 °C. It correlates well with the FBRM results and indicates that the precipitation was not completed when ending at pH 9 at 25 °C. Sun et al. (2012) stated that the end pH value should be controlled within a range of 9.0–9.5 to obtain a higher yield in the reaction of LiOH and $CO_2$, since pH is the direct reflection of the carbonation process. This is of considerable importance because carbonate speciation is highly dependent on the pH level. However, they did not mention at which temperature the pH should be controlled within the range of 9.0–9.5. This is slightly different from the observations in the current study that indicate that a favorable end pH is 8 for both temperatures. Therefore, the end pH should correspond to the specific system and temperature.

#### 3.1.3. Effect of mixing rate

Two mixing rates were investigated: 500 rpm and 600 rpm. At a constant flow rate of $CO_2$ and temperature, similar trends for pH and conductivity over time were obtained for both mixing rates, as shown in Fig. 2. It was found that the pH and conductivity reduced faster with a mixing rate of 600 rpm than with 500 rpm, which means that a higher mixing rate enhances the $CO_2$ absorption and chemical reaction, and thus promotes the nucleation and crystal growth in the precipitation process.

Fig. 4 shows that the particle size was smaller when the mixing rate was higher for both temperatures at a constant gas flow rate. This is because smaller bubbles are generated with a higher mixing intensity, which increases the interfacial area between gas and liquid. Therefore, higher supersaturation was generated, enhancing the absorption and chemical reaction, and resulting in the formation of small particles.

#### 3.1.4. Characterization of $Li_2CO_3$ precipitates

All the final precipitates obtained from precipitation were identified by XRD. Typical XRD patterns of the $Li_2CO_3$ particles are shown in Fig. 5. All samples correlate with reference data (ICDD 00–022-1141), which indicates that the $Li_2CO_3$ anhydrate mainly crystallized from the precipitation stage. The shape of the XRD peak demonstrates that the $Li_2CO_3$ is well crystallized. Fig. 6 illustrates the morphology of the precipitated $Li_2CO_3$ crystals. It can be seen that the $Li_2CO_3$ particles were present as massive agglomerates of leaf-shaped clusters. The crystals obtained at 25 °C have a cluster of elongated leaf-shaped sheets and the agglomerates are smaller, whereas the crystals obtained at 50 °C are larger in size with clusters of elliptoid-shaped sheets. The phenomenon is consistent with the results obtained from PSD measurements. Li et al. (2017) synthesized $Li_2CO_3$ with LiCl solution and $CO_2$ through a solvent extraction process and obtained flaky, flower-like, and nanorod particles. The flower-like particles in the reference (Li et al., 2017) were exactly the same as the crystals obtained in our previous study (Han et al., 2018) using LiCl and $Na_2CO_3$ solutions. Yang et al. (2018) recovered high purity $Li_2CO_3$ crystals having agglomerates of bar-shaped particles after selective leaching from spent $LiFePO_4$ batteries. However, their morphologies differ from the precipitated $Li_2CO_3$ obtained in the present work. This may be due to the existence of additional ions or impurities, which can affect nucleation and crystal growth during the precipitation process.

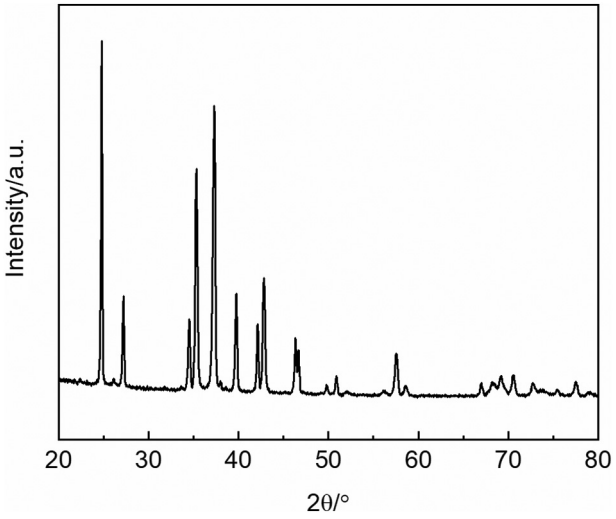


**Fig. 5.** Typical XRD patterns of $Li_2CO_3$ crystals.

### 3.2. Homogeneous precipitation

Semi-batch homogeneous precipitation experiments were carried out with two different stirring speeds (500 and 600 rpm) and three different feed rates (2.54, 4.42, and 5.65 mL/min; i.e., residence time 42, 24, and 19 min) at 50 °C.

#### 3.2.1. Effect of feed rate

Fig. 7 shows the pH and conductivity trends versus time at a mixing speed of 600 rpm with three different feed rates. The initial pH of the $Li_2SO_4$ solution has little variation due to the impurities present in the $Li_2SO_4$ chemical, which was previously discussed in Section 3.1. This may be the reason why the final pH of each experiment differs to some extent. Additionally, it makes difficult to compare the pH changes for different rotation speeds at a constant temperature and feed rate. As a summary, it seems that the gas-liquid thermodynamics between carbon dioxide and ionic carbonates and their chemical reactions in shifting pH conditions make the solution chemistry complex.

It can be seen from the pH trends in Fig. 7 that the pH increased sharply in the initial period of feeding the saturated solution of $Na_2CO_3$. Then it increased gradually until the endpoint where the pumping of saturated $Na_2CO_3$ solution was stopped. Finally, the pH remained constant during the aging period. The continuous increase in the pH during the reaction period between $Li^+$ and $CO_3^{2-}$ is because the saturated solution of $Na_2CO_3$ is an alkaline solution with a high pH of 12.02 measured by the pH electrode at 50 °C. The conductivity shown in Fig. 7 increased continuously until all of the saturated solution of $Na_2CO_3$ had been pumped to the reactor and until the end of the precipitation reaction between carbonate and lithium ions. After that, a slight decrease in conductivity occurred and then remained unchanged for the final aging period. This is because the addition of sodium carbonate solution increases the electric conductivity. The turning points of pH and conductivity during the chemical reaction period correspond to the three residence times, such as 19, 24, and 42 min, as shown in Fig. 7. The pH and conductivity changes for the experiments carried out with a stirring speed of 500 rpm at 50 °C and three different pumping rates were similar to those studied with a stirring speed of 600 rpm, as shown in Fig. 7.

Fig. 8 provides information of the count rates together with the pH changes for the precipitation carried out at 600 rpm and 50 °C with feed rates of 5.65 and 2.54 mL/min. The count rates of < 10 μm start to increase at around 2.8 min (Fig. 8a) and 5.1 min (Fig. 8b) for the pumping rate of 5.65 and 2.54 mL/min, respectively. This indicates the nucleation of the $Li_2CO_3$ particles. This phenomenon is consistent with

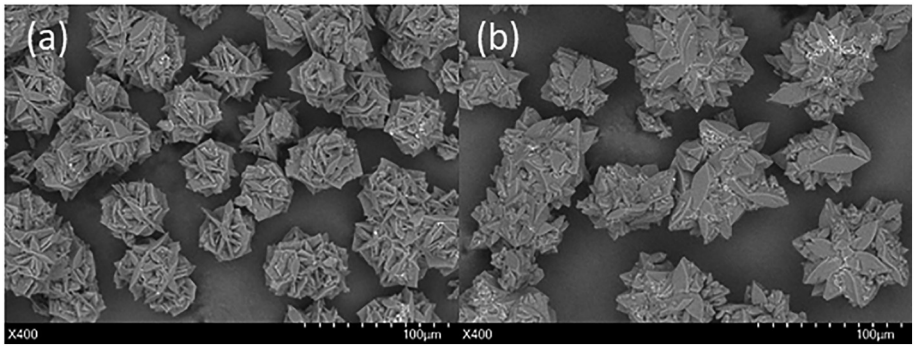


**Fig. 6.** Characteristic SEM images of precipitated $Li_2CO_3$ obtained at 25 °C (a) and 50 °C (b).

observations made with the naked eye, as indicated by the blue lines in Fig. 8. The count rates of size fractions below 10 μm and between 10 and 100 μm then rise rapidly, indicating that nucleation and crystal growth rate increase during the $Li_2CO_3$ precipitation process. The reaction shown in Eq. 4 continuously occurs during this period. After adding the saturated solution of $Na_2CO_3$, the count rates of < 10 and 10–100 μm almost maintain a certain level for the final aging period, which shows the stabilization of the whole system. All the other experiments operated with different conditions have similar trends for the count rates.

Particle size distributions of all the precipitates are shown in Fig. 9. No significant difference can be observed from the particles obtained at 500 rpm with the three pumping rates. Only a slight difference of PSD can be seen for the particles obtained with different feed rates at 600 rpm. Larger particles were formed with a higher feed rate, which indicates that stronger aggregation occurred with higher supersaturation.

### 3.2.2. Effect of rotation speed

Due to the presence of impurities in the $Li_2SO_4$, there was a slight difference in the initial pH of the solution and final pH of the system, as mentioned above. Thus, it is a considerable challenge to compare the pH changes for different rotation speeds at a constant temperature and feed rate. As seen in Fig. 9, the particles obtained at 500 rpm are larger than the particles precipitated at 600 rpm for different feed rates. This means that higher speeds can enhance the chemical reaction and weaken the aggregation, thus resulting in smaller particles.

### 3.2.3. Characterization of $Li_2CO_3$ crystals

The crystals obtained from homogeneous precipitation were examined by XRD. The results indicate that the $Li_2CO_3$ was mainly precipitated, corresponding to the reference data (ICDD 00–022-1141), as discussed in Section 3.1.4. The SEM images of the precipitated $Li_2CO_3$ crystals revealed that similar clusters of elliptoid-shaped sheets as shown in Fig. 6b were formed at 50 °C.

## 3.3. Comparison of heterogeneous and homogeneous precipitation of $Li_2CO_3$

As discussed in Section 3.1 and 3.2, heterogeneous and homogeneous precipitation were investigated in a stirred crystallizer. In general, the morphology of the $Li_2CO_3$ crystals precipitated at 50 °C is the same for both homogeneous and heterogeneous precipitation. The pH and conductivity changes over time are completely different, however, which indicates the differences in precipitation kinetics for homogeneous and heterogeneous precipitation. For heterogeneous precipitation, several steps are included, such as the absorption of carbon dioxide gas into the liquid phase, chemical reactions, and precipitation, which occurred simultaneously. The mass transfer of gas-liquid plays an important role, and has a significant impact on the following procedures. For homogeneous precipitation, however, only chemical reaction and precipitation are involved. The lithium recovery was calculated based on the mass of the dried crystals. In heterogeneous precipitation, the recovery of lithium is in the range of 41.6–45.5% and 22.6–25.6% for 50 °C and 25 °C, respectively. As stated in the reference (Sun et al., 2012), temperature is the most significant factor deciding the crystal yield. Usually the solubility of $CO_2$ decreases with an

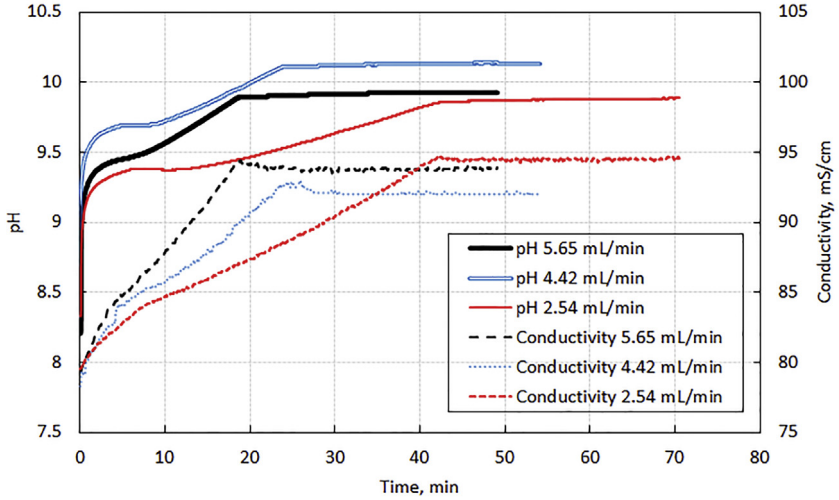


**Fig. 7.** Changes in pH and conductivity profiles as a function of time at a mixing rate of 600 rpm for different feed rates of saturated $Na_2CO_3$ solution at 50 °C in the homogeneous $Li_2CO_3$ precipitation process.

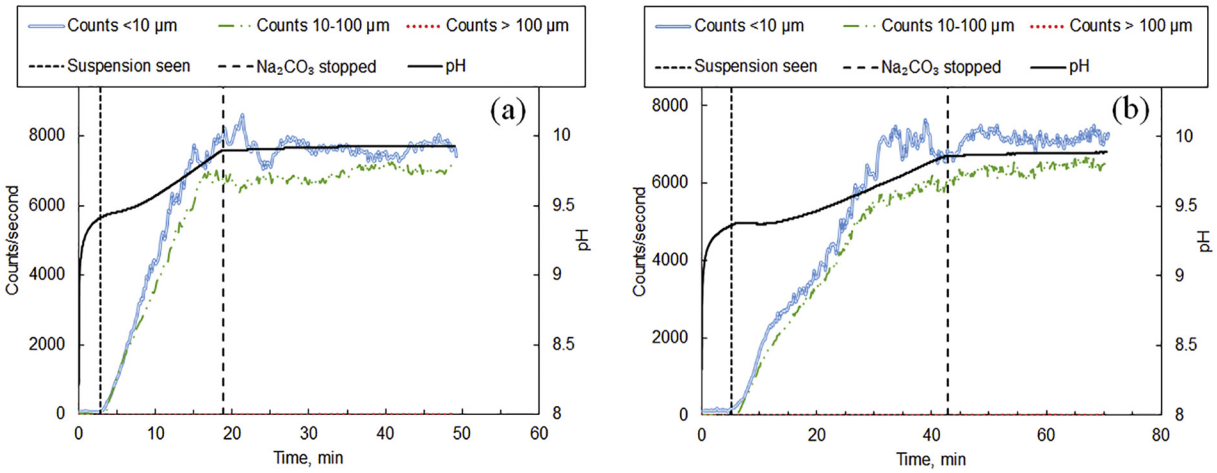


**Fig. 8.** Focused beam reflectance measurement (FBRM) signal and pH trends over time at a mixing rate of 600 rpm and constant temperature of 50 °C for the feed rate of 5.65 mL/min (a) and 2.54 mL/min (b) in the homogeneous $Li_2CO_3$ precipitation process.

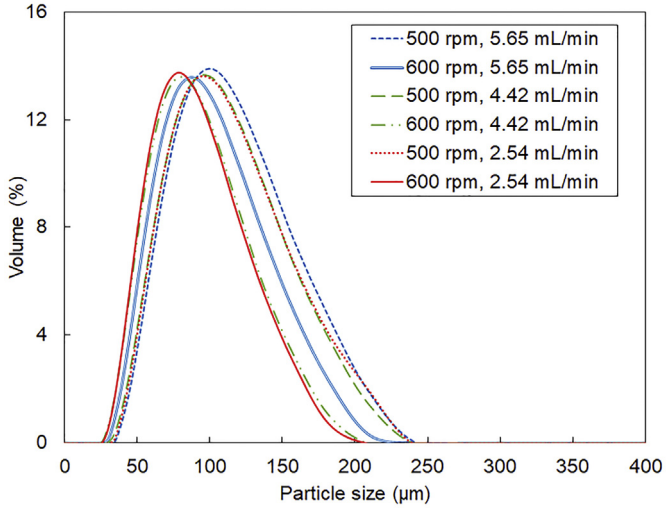


**Fig. 9.** Particle size distribution of $Li_2CO_3$ obtained from the various mixing and feed rates of $Na_2CO_3$ in the homogeneous precipitation process.

increase of temperature. However, in the current complex heterogeneous precipitation process, supersaturation and precipitation kinetics are significantly enhanced with a certain rise of temperature. Moreover, the chemical reaction rate is accelerated with the increase of temperature, since a high temperature can increase the chance of collision between different ions and increase the number of active molecules (Zhao et al., 2019a, 2019b). In homogeneous precipitation, the lithium recovery is around 72.3% to 75.6% at 50 °C. In practice, there are deviations in these recoveries since crystals cannot be fully emptied from the crystallizer. However, it can be seen that higher lithium recovery can be reached with homogeneous precipitation. From another point of view, the theoretical recovery of lithium for homogeneous precipitation is 87.8% at 50 °C. As the mechanism and kinetics of the heterogeneous precipitation studied have not been investigated comprehensively, the theoretical recovery of lithium was calculated based on the assumption that the $CO_3^{2-}$ formed originated from the capture of $CO_2$ with the amount of NaOH added to the system, i.e., 45.6% and 41.9% for 50 °C and 25 °C, respectively. Therefore, the lithium recovery obtained at 50 °C in the current study is quite close to the theoretical value for heterogeneous precipitation, even though the recovery was very low. The recovery obtained in the present work with heterogeneous precipitation at 25 °C is much lower than the theoretical value. This may be because the precipitation was not completed at the final pH value of 9 at 25 °C. Another reason is that the solubility of $Li_2CO_3$ is higher at lower temperatures.

Due to the difficulties in controlling the initial pH of the $Li_2SO_4$ solution, the residence time used in heterogeneous precipitation varied. The residence time of the heterogeneous experiment carried out at 50 °C, 600 rpm, and a gas flow rate of 0.3 L/min was 23.3 min, which is quite similar to the homogeneous experiment operated at 50 °C, 600 rpm, and a $Na_2CO_3$ feed rate of 4.42 mL/min, which had a residence time of 24 min. Thus it was decided to use these two experiments for a specific comparison. Fig. 10 shows the comparison of the experiments. It can be seen that the $Li_2CO_3$ particles obtained from heterogeneous precipitation are larger than the particles obtained from homogeneous precipitation. The median size of the particles is 82 μm and 74 μm for heterogeneous and homogeneous precipitation, respectively. The reason may be the gas bubbles generated were very large, since the $CO_2$ gas was introduced through eight 1-mm diameter holes in the sparger, even though a high speed of 600 rpm was used. Therefore, the particles formed were relatively larger than those formed from homogeneous precipitation.

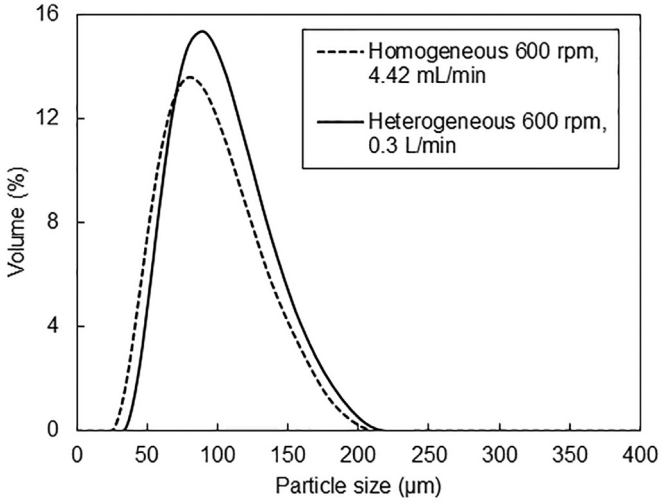


**Fig. 10.** Comparison of particle size distribution of $Li_2CO_3$ crystals obtained from homogeneous and heterogeneous precipitation with a similar residence time at 50 °C and 600 rpm. Residence times were 24 min with a feed rate of 4.42 mL/min in the homogeneous reaction, and 23.3 min with a gas flow rate of 0.3 L/min in the heterogeneous reaction.

## 4. Conclusions

Semi-batch precipitation of $Li_2CO_3$ was carried out by heterogeneous reaction using $CO_2$ and by homogeneous reaction with aqueous $Na_2CO_3$ solution in the same crystallizer. The effects of temperature, gas flow rate, and mixing speed on heterogeneous precipitation and the impacts of the pumping rate and mixing speed on homogeneous precipitation were investigated. Well-shaped $Li_2CO_3$ was mainly crystallized from both the heterogeneous and homogeneous experiments, and was examined by XRD. The flower-like particles were composed of massive agglomerates of leaf-shaped primary crystallites. The primary crystals obtained from 25 and 50 °C present a slight difference in heterogeneous or homogeneous precipitation, which means that the shape of the primary crystals obtained from 50 °C is elliptoid, whereas elongated sheets as primary crystals were formed at 25 °C. Moreover, it was found that nucleation and crystal growth can be monitored easily and accurately for homogeneous and heterogeneous precipitation with inline Particle Track.

The results obtained from the heterogeneous reaction indicate that the final pH and temperature play important roles in the precipitation process. The final pH value should reach 8 to stop the input of $CO_2$ at 25 and 50 °C, which can ensure the process of achieving equilibrium state. This was proved by the FBRM count rates of various size fractions measured by inline Particle Track. A smaller particle size can be obtained with a higher rotation speed since higher supersaturation was achieved with the formation of small bubbles that accelerate the chemical reaction. No significant influence of the gas feed rate on the particle size was observed. Particles were larger with the higher temperature. An almost doubled crystal yield can be obtained with a temperature of 50 °C in the heterogeneous reaction with $CO_2$.

In contrast, for homogeneous precipitation, the particle size was smaller with the higher rotation speed, which is the same as the conclusion made for heterogeneous precipitation. However, the pumping rate of $Na_2CO_3$ solution did not have a significant impact on the particle size.

In the comparison of homogeneous and heterogeneous reactions studied in the present work, the crystal yield is higher with homogeneous precipitation. This is because a higher concentration of $CO_3^{2-}$ was provided by the saturated solution of $Na_2CO_3$ in homogeneous precipitation. In the heterogeneous reaction, however, the formation of $CO_3^{2-}$ was controlled by the adsorption of mass transfer. It should be noted that a high alkaline concentration is needed to induce the precipitation of $Li_2CO_3$ by using $CO_2$ from $Li_2SO_4$ solution.

The current work clearly shows that using $CO_2$ in heterogeneous reactive crystallization and using $Na_2CO_3$ in homogeneous reactive crystallization can be feasible ways to recover lithium as lithium carbonate salt from $Li_2SO_4$ solution. To improve the recovery of lithium, solids of $Na_2CO_3$ can be considered for use in homogeneous precipitation since the volume of the whole solution is not increased by adding $Na_2CO_3$ solids. The crystal size and morphology should be carefully considered in this case. The residue of the mother liquor from both precipitation processes can be further used to precipitate more poorly soluble salts such as $Li_3PO_4$. The application of $CO_2$ to recover lithium would bring considerable value as a contribution to the circular economy and sustainability. Further research work is definitely needed to improve the yield and crystal purity. Applying inline technical tools such as an inline camera and Raman spectroscopy would provide information on real-time changes in the $CO_3^{2-}$ and $HCO_3^-$ concentration, solids formation and morphology, thereby providing a deeper understanding of precipitation kinetics.

## Acknowledgments

The authors would like to thank Ms. Camille Breemeersch for her contribution to the experimental work. This research did not receive any specific grant from funding agencies in the public, commercial, or not-for-profit sectors.

## Declarations of interest

None.

## References

CRC Handbook of Chemistry and Physics, Haynes W. (Ed.), 91th ed.; CRC press, 2010-2011.

Ferrini, V., Vito, C.D., Mignardi, S., 2009. Synthesis of nesquehonite by reaction of gaseous $CO_2$ with Mg chloride solution: its potential role in the sequestration of carbon dioxide. J. Hazard. Mater. 168, 832–837. https://doi.org/10.1016/j.jhazmat.2009.02.103.

Flixer, V., Baspineiro, C.F., Galli, C.I., 2018. Lithium recovery from brines: a vital raw material for green energies with a potential environmental impact in its mining and processing. Sci. Total Environ. 639, 1188–1204. https://doi.org/10.1016/j.scitotenv.2018.05.223.

Han, B., Louhi-Kultanen, M., 2018. Real-time Raman monitoring of calcium phosphate precipitation in a semi-batch stirred crystallizer. Cryst. Growth Des. 18, 1622–1628. https://doi.org/10.1021/acs.cgd.7b01587.

Han, B., Qu, H., Niemi, H., Sha, Z., Louhi-Kultanen, M., 2014. Mechanistic study of magnesium carbonate semibatch reactive crystallization with magnesium hydroxide and $CO_2$. Ind. Eng. Chem. Res. 53, 12077–12082. https://doi.org/10.1021/ie501706j.

Han, B., Porvali, A., Lundström, M., Louhi-Kultanen, M., 2018. Lithium recovery by precipitation from impure solutions-lithium ion battery waste. Chem. Eng. Technol. 41 (6), 1205–1210. https://doi.org/10.1002/ceat.201700667.

Li, L., Sui, J., Huang, R., Xiang, W., Qin, W., 2017. Dependence of electrochemical properties of spinel $LiMn_2O_4$ on $Li_2CO_3$ with micro-flaky, micro-flower and nanorod morphologies. RSC Asv. 7, 42289–42295. https://doi.org/10.1039/c7ra07088h.

Litio, F.Jimenez, D. Lithium market outlook. http://s1.q4cdn.com/793210788/files/doc_news/2018/6/Foro-del-Litio-2018-Lithium-Market-Update-20180808-FINAL.pdf.

Matsumoto, M., Morita, Y., Yoshinaga, M., Hirose, S., Onoe, K., 2009. Reactive crystallization of lithium carbonate nanoparticles by microwave irradiation of aqueous solution containing $CO_2$ microbubbles. J. Chem. Eng. Japan 42, s242–s248. https://doi.org/10.1252/jcej.08we173.

Meng, F., McNeice, J., Zadeh, S.S., Ghahreman, A, 2019. Review of lithium production and recovery from minerals, brines, and lithium-ion batteries. Mineral Processing and Extractive Metallurgy Review 1–19. https://doi.org/10.1080/08827508.2019.1668387.

Nayl, A.A., Elkhashab, R.A., Badawy, S.M., El-Khateeb, M.A., 2017. Acid leaching of mixed spent Li-ion batteries. Arab. J. Chem. 10, S3632–S3639. https://doi.org/10.1016/j.arabjc.2014.04.001.

Sun, Y., Song, X., Wang, J., Yu, J., 2012. Preparation of $Li_2CO_3$ by gas-liquid reactive crystallization of LiOH and $CO_2$. Cryst. Res. Technol. 47 (4), 437–442. https://doi.org/10.1002/crat.201100571.

Swain, B., 2017. Recovery and recycling of lithium: a review. Sep. Purif. Technol. 172, 388–403. https://doi.org/10.1016/j.seppur.2016.08.031.

Swain, B., 2018. Cost effective recovery of lithium from lithium ion battery by reverse osmosis and precipitation: a perspective. J. Chem. Technol. Biotechnol. 93, 311–319. https://doi.org/10.1002/jctb.5332.

Velts, O., Uibu, M., Kallas, J., Kuusik, R., 2011. Prospects in waste oil shale ash sustainable valorization. World Acad. Sci. Eng. Technol. 52, 451–455.

Whittingham, M.S., 2004. Lithium batteries and cathode materials. Chem. Rev. 104, 4271–4301. https://doi.org/10.1021/cr020731c.

Xu, Z., Zhang, H., Wang, R., Gui, W., Liu, G., Yang, Y., 2014. Systemic and direct production of battery-grade lithium carbonate from a saline lake. Ind. Eng. Chem. Res. 53, 16502–16507. https://doi.org/10.1021/ie502749n.

Yang, Y., Meng, X., Cao, H., Lin, X., Liu, C., Sun, Y., Zhang, Y., Sun, Z., 2018. Selective recovery of lithium from spent lithium iron phosphate batteries: a sustainable process. Green Chem. 20, 3121–3133. https://doi.org/10.1039/c7gc03376a.

Zhang, P.W., Yokoyama, T., Itabashi, O., Suzuki, T.M., Inoue, K., 1998. Hydrometallurgical process for recovery of metal values from spent lithium-ion secondary batteries. Hydrometallurgy 47, 259–271. https://doi.org/10.1016/S0304-386X(97)00050-9.

Zhao, C., Zhang, Y., Cao, H., Zheng, X., Gerven, T.V., Hu, Y., Sun, Z., 2019a. Lithium carbonate recovery from lithium-containing solution by ultrasound assisted precipitation. Ultrasonics-Sonochemistry 52, 484–492. https://doi.org/10.1016/j.ultsonch.2018.12.025.

Zhao, C., Zhang, Y., Cao, H., Zheng, X., Gerven, T.V., Hu, Y., Sun, Z., 2019b. Dataset of lithium phosphate recovery from a low concentrated lithium-containing solution. Data in Brief 25, 104044. https://doi.org/10.1016/j.dib.2019.104044.

Zhou, Z., Liang, F., Qin, W., Fei, W., 2014. Coupled reaction and solvent extraction process to form $Li_2CO_3$: mechanism and product characterization. AIChE 60, 282–288. https://doi.org/10.1002/aic.14243.

Report on Critical Raw Materials for the EU. Report of the Ad Hoc Working Group on Defining Critical Raw Materials. http://ec.europa.eu/DocsRoom/documents/10010/attachments/1/translations, Accessed date: 10 Oct. 2019.